First, the conventional, rapid expansion gas dynamic laser[3-5] creates a population inversion between the (001) and (100) levels in CO_2 which subsequently lases at $\lambda = 10.6\mu$. In contrast, the inversions shown in Fig. 4 between the (04°0) and (001) levels, and between the (200) and (001) levels, would correspond to laser transitions at 50μ and 22μ, respectively. An important parameter for gas lasers is small signal gain, G_0, defined as $dI/I = G_0 dz$ where I is the incident radiation intensity on a slab of laser gas of thickness dz, and dI is the increase in beam intensity after traversing the length dz. As shown in Appendix A of Ref. 15, $G_0 \propto (\lambda^2/\tau_{21}) \cdot IN \propto (M^2/\lambda) \cdot IN$, where τ_{21} is the spontaneous radiative lifetime for a transition between the upper and lower laser levels, M is the corresponding quantum mechanical matrix element, and IN is the population inversion. For CO_2, computed values of M for the 50μ, 22μ, and 10.6μ transitions are in the ratio $0.21 \times 10^{-2}:0.21\times10^{-2}:0.34 \times 10^{-1}$, respectively.[16] Also, the shock induced population inversions shown in Fig. 4 are approximately one order of magnitude smaller than typical inversions created in rapid expansions through supersonic nozzles. In light of the above numbers, a comparison of G_0 at 50μ and 22μ behind a shock wave with G_0 at 10.6μ in a rapid expansion leads to $(G_0)_{50\mu}/(G_0)_{10.6\mu} \approx 10^{-4}$ and $(G_0)_{22\mu}/(G_0)_{10.6\mu} \approx 2 \times 10^{-4}$. Clearly, the nonequilibrium region behind a normal shock wave in CO_2–N_2–He mixtures produces a low-gain medium. A more detailed discussion and comparison of these and other laser properties are contained in Ref. 14.

Conclusion

The present study indicates that population inversions occur behind a normal shock front due strictly to translation-vibration and vibration-vibration molecular energy exchanges in CO_2–N_2–He mixtures. However, the laser properties of this shock-induced nonequilibrium flow are clearly not as promising as those of gas dynamic lasers operating on the principle of rapid expansion.

References

[1] Basov, N. G. and Oraevskii, A. N., "Attainment of Negative Temperatures by Heating and Cooling of a System," *Soviet Physics JETP*, Vol. 17, No. 5, Nov. 1963, pp. 1171–1172.

[2] Hurle, I. R. and Hertzbeg, A., "Electronic Population Inversions by Fluid—Mechanical Techniques," *The Physics of Fluids*, Vol. 8, No. 9, Sept. 1965, pp. 1601–1607.

[3] Gerry, E. T., "Gasdynamic Lasers," AIAA Paper 71-23, New York, 1971.

[4] Hertzberg, A. et al., "Photon Generators and Engines for Laser Power Transmission," AIAA Paper 71-106, New York, 1971.

[5] Anderson, J. D., Jr. and Winkler, E. M., "High Temperature Aerodynamics with Electromagnetic Radiation," *Proceedings of the IEEE*, Vol. 59, No. 4, April 1971, pp. 651–658.

[6] Oraevskii, A. N., "Population Inversion Obtained by Thermal Dissociation of Molecules in a Shock Wave," *Soviet Physics JETP*, Vol. 21, No. 4, Oct. 1965, pp. 768–770.

[7] Gross, R. W. F. et al., "Stimulated Emission Behind Overdriven Detonation Waves in F_2O-H_2 Mixtures," *Journal of Chemical Physics*, Vol. 51, No. 3, Aug. 1969, p. 1250.

[8] Anderson, J. D., Jr., "A Time-Dependent Analysis of Population Inversions in an Expanding Gas," *The Physics of Fluids*, Vol. 13, No. 8, Aug. 1970, pp. 1983–1989.

[9] Taylor, R. L. and Bitterman, S., "Survey of Vibrational Relaxation Data for Processes Important in the CO_2–N_2 Laser System," *Reviews of Modern Physics*, Vol. 41, No. 1, Jan. 1969, pp. 26–47.

[10] MacDonald, J. R., private communication, Jan. 20, 1971, Max-Planck-Institut Fur Plasmaphysik, Garching Bei Munchen, West Germany.

[11] Lee, G. and Gowan, F. E., "Gain of CO_2 Gasdynamic Lasers," *Applied Physics Letters*, Vol. 18, No. 6, March 15, 1971, pp. 237–239.

[12] Christiansen, W. H., and Tsongas, G. A., "Gain Kinetics of High Pressure Gasdynamic Lasers," Univ. of Washington (submitted for publication in *The Physics of Fluids*).

[13] Madden, M. T., Anderson, J. D., Jr., and Piper, C. H., "Equilibrium Normal Shock Properties for Vibrationally Excited CO_2–N_2–He Mixtures," NOLTR 70-103, May 1970, U.S. Naval Ordnance Lab., White Oak, Md.

[14] Anderson, J. D., Jr., Madden, M. T., and Piper, C. H., "Vibrational Population Inversions Behind Normal Shock Waves in CO_2–N_2–He Mixtures," NOLTR 70-214, Oct. 1970, U. S. Naval Ordnance Lab., White Oak, Md.

[15] Anderson, J. D., Jr., "Numerical Experiments Associated with Gas Dynamic Lasers," NOLTR 70-198, Sept. 1970, U.S. Naval Ordnance Lab., White Oak, Md.

[16] Lalos, G., private communication, Aug. 6, 1970, U.S. Naval Ordnance Lab., White Oak, Md.

Computation of Incompressible Turbulent Boundary Layers at Low Reynolds Numbers

TUNCER CEBECI* AND G. J. MOSINSKIS†

Douglas Aircraft Company, Long Beach, Calif.

Introduction

CURRENTLY there are several quite accurate numerical methods for calculating turbulent boundary layers. Some of these methods are based on the solution of the momentum integral and/or energy integral equations and are called integral methods. Other methods are based on the solution of the governing conservation equations in their partial-differential equation form. These are called differential methods. Almost all these prediction methods are based on empirical data obtained at high Reynolds numbers ($R_\theta > 6000$). According to several experiments and investigators there is a definite Reynolds effect for $R_\theta < 6000$. For example, in Ref. 1, Coles observed that his law of the wall formulation failed for low Reynolds numbers; the strength of the wake component, which stayed constant for momentum Reynolds numbers greater than 6000, showed a large variation at low Reynolds numbers. It should, however, be mentioned that Coles' analysis relies on the constancy of k and c in the logarithmic velocity profile.

$$u^+ \equiv u/u_\tau = 1/k \ln(yu_\tau/\nu) + c, \quad u_\tau \equiv (\tau_w/\rho)^{1/2} \quad (1)$$

The low Reynolds number effect is quite important in turbomachines and on airfoils in wind tunnels. For example,

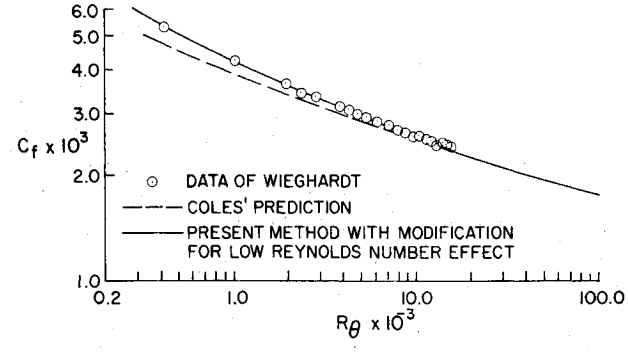

Fig. 1 Calculated and experimental skin-friction coefficients for a flat-plate turbulent flow at low Reynolds numbers.

Received February 8, 1971; revision received March 29, 1971. This research was supported by the Naval Ship Research and Development Center under Contract N00014-70-C-0099, Subproject SR 009 01 01.

Index Category: Boundary Layers and Convective Heat Transfer–Turbulent.

* Senior Engineer/Scientist, Aerodynamics Research. Member AIAA.

† Engineer/Scientist, Aerodynamics Research. Member AIAA.

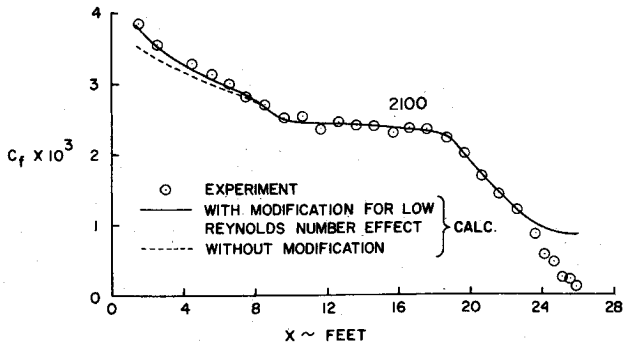

Fig. 2 Calculated and experimental skin-friction coefficients for a flow with pressure gradient, case 2100 (data of Schubauer and Klebanoff).

in calculating the viscous drag of airfoils at chord Reynolds numbers R_c ranging from 3–9 $\times$ 10^6, the momentum-thickness calculation of drag depends mostly upon the accuracy of calculating turbulent boundary layers from the point of transition.

This Note presents one approach by which the eddy-viscosity and mixing-length concepts that are being used in the current differential methods can be modified to calculate incompressible turbulent boundary layers at low Reynolds numbers. A comparison of several calculated results using this modification shows good agreement with experiment.

Analysis

We consider the momentum equation

$$u\partial u/\partial x + v\partial u/\partial y = -(1/\rho)dp/dx + (1/\rho)\partial\tau/\partial y \quad (2)$$

and the eddy-viscosity formulation of Ref. 2, which for inner and other regions of the boundary layer is defined by ϵ_i and ϵ_0, respectively,

$$\epsilon = \begin{cases} \epsilon_i = (ky)^2[1 - \exp(-y/A)]^2 \left|\dfrac{\partial u}{\partial y}\right| & 0 \le y \le y_c \\ \epsilon_0 = 0.0168 \left|\displaystyle\int_0^\infty (u_e - u)dy\right| [1 + 5.5\ (y/\delta)^6]^{-1} & y_c \le y \le \delta \end{cases} \quad (3)$$

In Eq. (2), τ is the total shear stress given by

$$\tau = \mu\, \partial u/\partial y - \rho\, \langle u'v' \rangle \quad (4)$$

and A in Eq. (3) is a damping-length constant given by

$$A = A\nu^+(\tau_w/\rho)^{-1/2}\{- p^+/v_w^+ [\exp\ (11.8\ v_w^+) - 1] + \exp(11.8\ v_w^+)\}^{-1/2} \quad (5)$$

where $p^+ = -(dp/dx)\nu/\rho u_\tau^3$, $v_w^+ = v_w/u_\tau$. The empirical constants k and A^+ appearing in Eqs. (2) and (5), which are given by 0.40 and 26, respectively, were obtained by Van Driest from experimental data at high Reynolds numbers. If we assume that these parameters change for flows at low

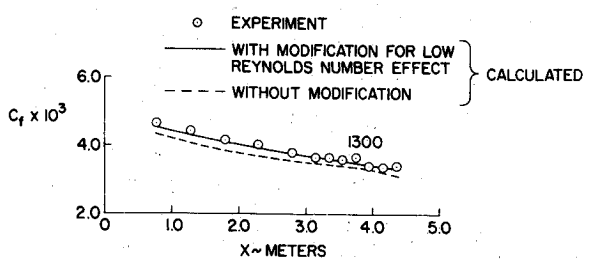

Fig. 3 Calculated and experimental skin-friction coefficients for a favorable pressure-gradient flow, case 1300 (data of Ludwieg and Tillmann).

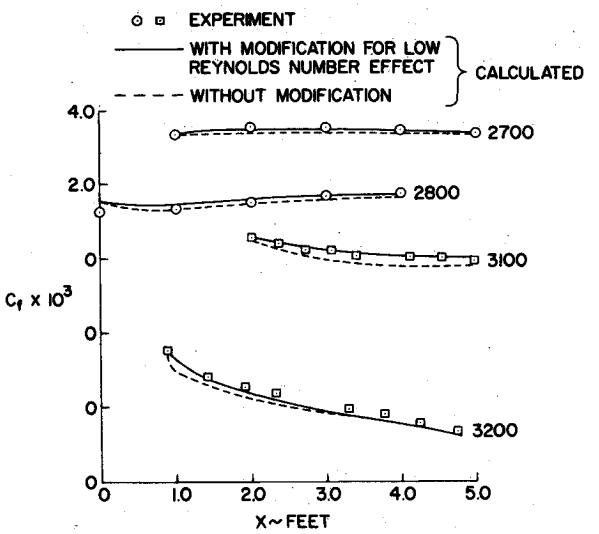

Fig. 4 Calculated and experimental skin-friction coefficients for flows with favorable and adverse pressure gradients, cases 2700, 2800 (data of Herring and Norbury), and 3100, 3200 (data of Bell).

Reynolds numbers, then this variation can be obtained by repeating Van Driest's procedure[3] for a flat-plate turbulent flow. Close to the wall, the momentum equation can be approximated by

$$d\tau/dy = 0 \quad \text{or} \quad \tau = \tau_w \quad (6)$$

Then by the concept of eddy viscosity, Eqs. (3) and (6) can be written as

$$\tau = \tau_w = \mu du/dy + \rho\epsilon du/dy \quad (7)$$

Substituting the inner eddy-viscosity expression in Eq. (3) into Eq. (7), it can be shown that Eq. (7) can be written as

$$du^+/dy^+ = 2/(1 + \{1 + 4k^2(y^+)^2[1 - \exp(- y^+/A^+)]^2\}^{1/2}) \quad (8)$$

Integrating Eq. (8) numerically for various values of k and A^+ for a given R_θ — flow and comparing the results with the experimental data, one can easily obtain the variation of these parameters with Reynolds number. For the experimental flat-plate data of Simpson[4] this curve-fitting procedure yields,

$$k = 0.40 + 0.19/(1 + 0.49z^2),$$
$$A^+ = 26 + 14/(1 + z^2) \quad z \ge 0.3 \quad (9)$$

where $z = R_\theta \times 10^{-3}$.

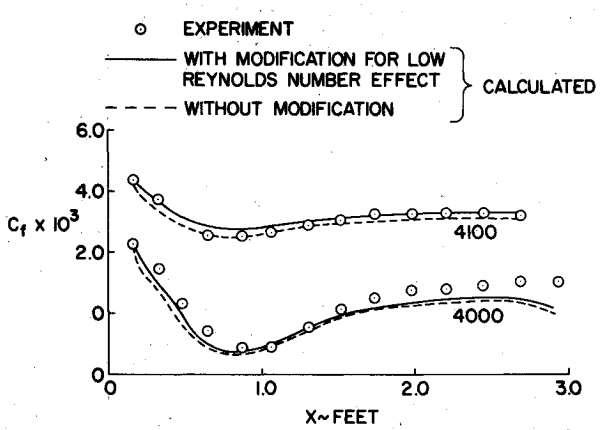

Fig. 5 Calculated and experimental skin-friction coefficients for flows with pressure gradient, cases 4000 and 4100 (data of Moses).

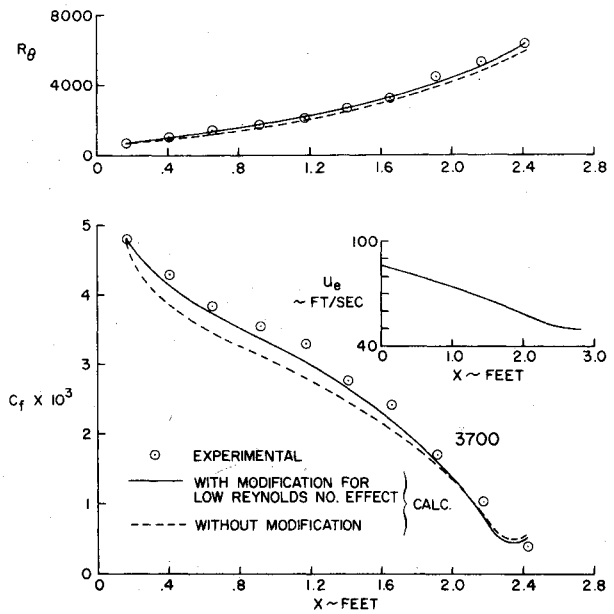

Fig. 6 Calculated and experimental results for case 3700 (data of Moses).

Comparison with Experiment

Figures 1–6 show a comparison of the calculated results with the experiment. The experimental data considered here correspond to the low Reynolds numbers given in Ref. 5. The calculations were made by using the method of Ref. 6, which for incompressible flows consists of solving Eqs. (2) and (3) together with the continuity equation. The method is applicable to both laminar and turbulent boundary layers. The calculations can be started either at the leading edge or at some downstream location. In the former case, the flow starts as laminar and becomes turbulent at any specified x-location by activating the eddy-viscosity expressions. In the latter case, it is necessary to specify the initial velocity profiles.

Figures 1–3 show the calculated and experimental results in which the calculations were started at the leading edge. In these calculations at first an effective length that matched the initial experimental momentum thickness was calculated. For flat-plate flows or flows with initially negligible pressure gradient, this procedure is a satisfactory one. Figure 1 compares the calculated c_f-values with those given by Coles' prediction[7] and the experimental values of Wieghardt.[5] Figure 2 shows the results for Schubauer and Klebanoff's airfoil-like body designated as 2100 in Ref. 5. It is seen that with the low Reynolds number correction, when the experimental R_θ is matched, the skin-friction coefficient is matched also. Figure 3 shows the results for an accelerating flow designated as 1300 in Ref. 5. Again when R_θ is matched, the skin-friction coefficient is also matched.

Figures 4–6 show the calculated and experimental results in which the calculations were started with the experimental initial velocity profile. Calculations were made for various flows with pressure-gradients designated as 2700, 2800, 3100, 3200, 3700, 4000 and 4100 in Ref. 5. As the results show, in all cases the Reynolds-number correction to the calculated results seems to improve the agreement with experiment.

References

[1] Coles, D. E., "The Turbulent Boundary Layer in a Compressible Fluid," Rept. P-2417, 1961, Rand Corp., Santa Monica, Calif.

[2] Cebeci, T., "The Behavior of Turbulent Flow Near a Porous Wall With Pressure Gradient," *AIAA Journal*, Vol. 8, No. 12, Dec. 1970, pp. 2152–2156.

[3] Van Driest, E. R., "On Turbulent Flow Near a Wall," *Journal of Aerospace Science*, Vol. 23, No. 11, Nov. 1956, pp. 1007–1011.

[4] Simpson, R. L., Kays, W. M., and Moffat, R. J., "The Turbulent Boundary Layer on a Porous Plate: An Experimental Study of the Fluid Dynamics With Injection and Suction," Rept. HMT-2, 1967, Stanford Univ., Stanford, Calif.

[5] Coles, D. E. and Hirst, E. H., eds., *Proceedings of the Computation of Turbulent Boundary Layers*, Stanford Univ., Vol. II, 1969.

[6] Cebeci, T. and Smith, A. M. O., "A Finite-Difference Method for Calculating Compressible Laminar and Turbulent Boundary Layers," *Journal of Basic Engineering*, Vol. 92, No. 3, Sept. 1970, pp. 523–535.

[7] Coles, D. E., "Measurements in the Boundary Layer on a Smooth Flat Plate in Supersonic Flow. I. The Problem of the Turbulent Boundary Layer," Rept. 20-69, June 1953, Jet Propulsion Lab., Pasadena, Calif.

Solar Electron Temperatures and X-Ray Flare Activity

D. M. Horan* and R. W. Kreplin†
Naval Research Laboratory, Washington, D. C.

Parameters of Solar X-Ray Source Regions

X-RAYS, especially in the shorter wavelengths, are not uniformly emitted from the solar disk, but have discrete, active regions as sources. Therefore, changes in the magnitude or spectral character of the solar energy flux must be associated with changes in the solar source regions.

The predominant source mechanisms for continuum solar x-ray emission are free-free (bremsstrahlung) transitions and free-bound (radiative recombination) transitions. Equations describing such transitions[1] show that the electron concentration, volume, and electron temperature associated with the source region are parameters which would affect the magnitude and spectral character of the solar x-ray emission. It is possible to use a pair of broad-band x-ray sensors to measure changes in these parameters and a brief outline of the technique follows.

The current generated in an ionization chamber is given by[2]

$$I = Ae\omega\int\epsilon(\lambda)E(\lambda,T)d\lambda \qquad (1)$$

where e is the electronic charge, ω is the number of ion pairs produced in the gas per unit of absorbed energy, A is the effective window area of the detector, $E(\lambda,T)$ is the solar emission spectrum, λ is the wavelength, T is the electron temperature, $\epsilon(\lambda)$ is the efficiency of the detector, and the integration is performed over wavelengths where ϵ is nonzero. If two ionization chambers sensitive to slightly different portions of the x-ray band are used, the ratio of the currents generated will be dependent on the electron temperature through the solar emission spectrum, $E(\lambda,T)$. If the solar emission spectrum is due to bremsstrahlung and radiative recombination, we are able to express it in the form

$$E(\lambda,T) = C(\lambda,T)\int N_e^2 dV \qquad (2)$$

Presented as Paper 70-1371 at the AIAA Observation and Prediction of Solar Activity Conference, Huntsville, Ala., November 16–18, 1970; submitted January 15, 1971; revision received March 26, 1971. The authors acknowledge the support of the Naval Air Systems Command under NAVAIR Air Task Number A3705381 652B 1F01551701, SOLRAD (Solar Radiation). Also, the authors gratefully acknowledge the assistance of K. P. Dere who spent a considerable amount of time searching for suitable data and converting it into a computer-compatible form.

* Research Physicist, E. O. Hulburt Center for Space Research.
† Head, Solar Radiation Section, Upper Air Physics Branch.